Vibration Energy Scavenging System With Maximum Power Tracking for Micropower Applications

Chao Lu, Chi-Ying Tsui, *Member, IEEE*, and Wing-Hung Ki, *Member, IEEE*

***Abstract*—In this work, we present a vibration-based energy scavenging system based on piezoelectric conversion for micropower applications. A novel maximum power point (MPP) tracking scheme is proposed to harvest the maximum power from the vibration system. A time-multiplexing mechanism is employed to perform energy harvesting and MPP tracking alternately. In the MPP tracking mode, a voltage reference that represents the optimal output voltage at the MPP is generated. A control unit then uses this reference to track the system operation around the MPP. The proposed system is capable of self-starting up without the help of an energy buffer. As a result, it is suitable for battery-less applications or when the energy buffer is completely drained. This tracking scheme has very small power overhead and is simple to implement in VLSI. Hence, it is especially applicable for micropower systems. The entire design was fabricated in a 0.35-μm CMOS process. Experimental results verified the proposed MPP tracking scheme and demonstrated the system operation. Measurement results show that the power harvesting efficiency of the electrical circuitry is higher than 90%.**

***Index Terms*—Battery-less, maximum power point (MPP) tracking, micropower, vibration energy harvesting.**

I. Introduction

MICROPOWER ubiquitous applications, such as pico-radio, smart dust, or wireless sensor network [1]–[3], that integrate the functions of sensing, computation, and communication to facilitate the interaction between human and the environment, are becoming more and more popular. These applications require high integration, compact volume, low cost, long lifetime, and maintenance-free operation. One of the design challenges in these systems is to provide the power supply without any maintenance overhead. The conventional option is to use electrochemical batteries. However, the extreme constraints on the system size limit the battery capacity. At the same time, for applications such as implantable devices or wireless sensor networks, it is not practical or cost-effective to recharge or replace the battery. Thus, battery integration poses a big limitation on wide deployment of these micropower applications.

One promising approach to overcome the limited energy availability problem in these miniature systems is to scavenge energy from the environment. Examples of ambient energy sources are light, thermal, vibration, radio frequency wave, and radiation. Among these sources, low level mechanical vibrations commonly occur in various household or industrial places and it is estimated that vibrations inherent in the environment can provide a power density of tens to hundreds of microwatts per cm^3 [4]–[6], which is sufficient for these micropower applications. In recent years, vibration energy scavenging systems have drawn much attention in the research community [4]–[8]. In [5], it was shown that most of the common low-level vibration sources (e.g., small microwave oven) are vibrating in fundamental frequencies which are usually below 200 Hz. In this work, we focus on the design of battery-less energy harvesting systems that harness low-level (i.e., output voltage range of the energy harvester is 0 V–6 V) and low-frequency (i.e., 0–200 Hz) vibration energy through piezoelectric conversion.

Since the vibration sources can be very unsteady, the feature of self-starting up is very crucial for battery-less systems. When there is no vibration or the vibration level is too weak to be harvested, the system will gradually dissipate all the energy previously stored in the energy buffer and stop working. If the system does not have an additional battery as the backup power source and also does not have the capability of self-starting up, then later when the vibration level becomes strong enough for harvesting again, the system cannot restart as there is no power left in the system and will die permanently.

Previous research works have shown that the output of a vibrating piezoelectric material is similar to an ac current source [7]–[11]. Therefore, an ac-dc rectifier is usually used to generate a dc power supply for the application loads. The instantaneous harvested power is greatly affected by both the vibration status (i.e., magnitude and frequency) and the rectifier output voltage. Given a vibration status, the rectifier has an optimal output voltage that is best matched to the given vibration status and corresponds to the maximum electrical power harvesting. Because the vibration status heavily depends on the environment where the application is deployed, it is often unsteady and varies from applications to applications and from time to time. Hence, the optimal voltage point is also changing. To maximally harvest the vibration power, we need to track the vibration status dynamically and adjust the energy harvester output voltage for best load matching.

Previous research has addressed the issue of maximizing the harvested electrical power. Several control and optimization schemes have been proposed in the literature [8]–[15]. In [8], a fixed-voltage band-band control scheme was implemented. The output voltage of the ac-dc rectifier was maintained between two fixed voltage levels using Schmitt triggers. This scheme

Manuscript received January 25, 2010; revised June 08, 2010; accepted July 25, 2010. Date of publication October 11, 2010; date of current version September 14, 2011.

C. Lu is with the Department of Electrical and Computer Engineering, Purdue University, West Lafayette, IN 47907 USA (e-mail: eeluchao@alumni.ust.hk).

C.-Y. Tsui and W.-H. Ki are with the Department of Electrical and Computer Engineering, Hong Kong University of Science and Technology, Clear Water Bay, Kowloon, Hong Kong (e-mail: eetsui@ust.hk; eeki@ece.ust.hk).

Color versions of one or more of the figures in this paper are available online at http://ieeexplore.ieee.org.

Digital Object Identifier 10.1109/TVLSI.2010.2069574

does not perform any vibration tracking and maximum power harvesting cannot be guaranteed. Ottman *et al.* proposed two maximum power point tracking schemes by using dc-dc converters in [9], [10]. Expensive circuit components [e.g., digital signal processor (DSP)] and computation-intensive control algorithms were employed to adaptively adjust the duty cycle of the dc-dc converters to match the load with the MPP. The design considerations of [9] and [10] are not for low voltage and micropower applications. The power overhead of these MPP tracking schemes is relatively large. For example, the reported power overhead of the tracking unit is 5.74 mW in [10]. Therefore, they are not very efficient for micropower applications. From this, we can see that in order to use piezoelectric conversion in micropower applications, it is imperative to develop a new maximum power point (MPP) tracking method that has ultra low power overhead and low-cost implementation. In [11], Lefeuvre *et al.* proposed a tracking scheme that regulates the averaged input resistance of a dc-dc converter to the load matching resistance of the energy harvesting device. However, this scheme does not actually perform tracking and is applicable only when the load matching resistance of the energy harvesting device is known in advance. For an energy harvesting device that has a cantilever structure, it usually operates in a narrow frequency band around its mechanical resonant frequency. The load matching resistance can be treated as a known constant. However, for an energy harvesting device that has a non-cantilever structure, this scheme is not applicable as the energy harvesting device may vibrate in a wide frequency range and the load matching resistance varies with the environment and time.

In this paper, we present a low-overhead MPP tracking scheme based on a time-multiplexing mechanism. This scheme is designed for general piezoelectric conversion and hence is not restricted to cantilever structures. This tracking scheme adaptively senses the vibration status and directly generates an optimal output reference voltage of the ac-dc rectifier for maximum power harvesting. The tracking power overhead is in the order of microwatts, which accounts for only a few percents of the total harvested electrical power. The proposed micropower energy harvesting system was fabricated using a 0.35-μm CMOS process. Measurements were carried out to verify the proposed MPP tracking scheme and demonstrate the system operation.

II. Overall System Description

Fig. 1 shows the block diagram of the proposed battery-less micropower vibration energy scavenging system. It consists of four major building blocks: the energy harvester, the vibration tracker, the control block, and the application load.

The energy harvester consists of an ac-dc rectifier and a storage capacitor C_S. The energy harvesting and vibration tracking are performed in a time-multiplexing manner, which is controlled by the switch S_0 driven by the tracking pulse Φ. When the tracking pulse is low, the piezoelectric material is connected to the energy harvester for normal energy harvesting. The current generated from the piezoelectric material flows into the storage capacitor for energy storage. When the tracking pulse is high, the piezoelectric material is connected to the vibration tracker. The vibration tracker senses the ambient vibration status and produces the voltage reference $V_{\mathrm{ref\_refreshed}}$, which represents the optimal output voltage value for the energy harvester to achieve maximum power harvesting.

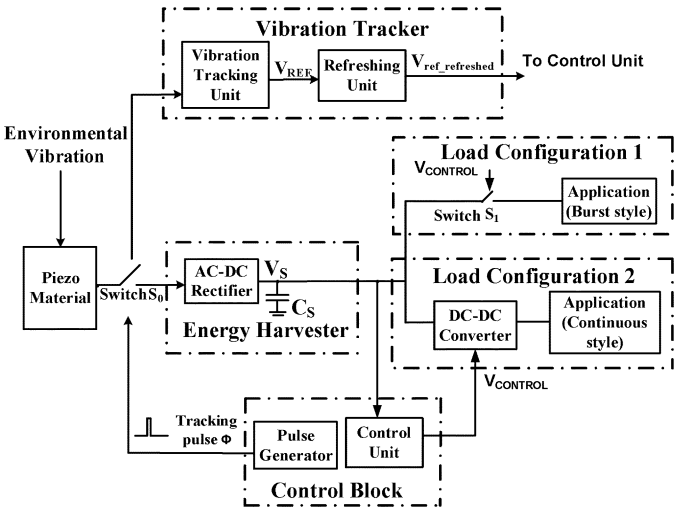

Fig. 1. Block diagram of the proposed energy harvesting system.

Inside the control block, a pulse generator is used to generate the tracking pulse Φ to control the time-multiplexing. The control unit compares the output voltage of the energy harvester (V_S) with the MPP reference voltage $(V_{\mathrm{ref\_refreshed}})$ to produce the control signal (V_{CONTROL}). The band-band control scheme is employed to maintain V_S around $V_{\mathrm{ref\_refreshed}}$ for load matching.

The energy harvesting system can support different load application scenarios. For applications that need continuous operation and a secondary energy buffer is available, the energy harvester can be connected to a dc-dc converter, which provides regulated output to charge up the energy buffer and at the same time acts as the load matching control. This scenario is similar to that used in vibration energy harvesting in [9] and [10] or in solar energy harvesting in [19] and [20]. This is shown in Fig. 1 as load configuration 2. Here, the control unit sends the V_{CONTROL} signal to the dc-dc converter to adaptively adjust its duty cycle to maintain V_S around $V_{\mathrm{ref\_refreshed}}$.

In other application situations where no secondary energy buffer is available, the application operates in a burst mode. The operation duty cycle depends on how much energy the system can harvest. The application switches between active mode and sleep mode depending on the harvested energy. To track the maximum harvested power, load matching is achieved by adaptively connecting the application load to the storage capacitor C_S through turning on and off the load switch S_1. When the energy stored in C_S is transferred to the application, the application will be triggered and woken up to start an atomic operation (e.g., sensing, data compression, and RF transmission). This is shown in Fig. 1 as load configuration 1. In this paper, we present and demonstrate our proposed vibration energy tracking scheme using the load configuration 1.

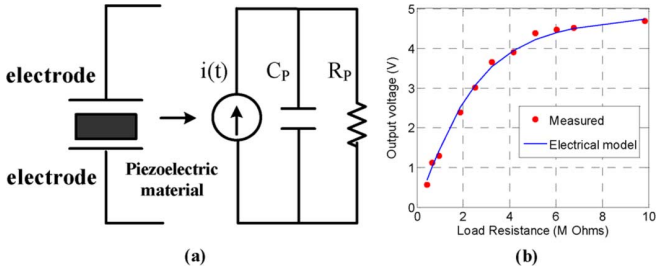

Fig. 2. Piezoelectric film model and experimental verification.

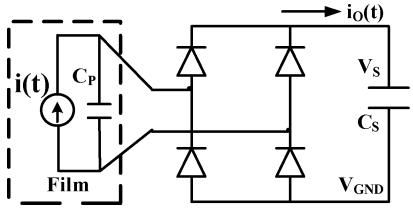

Fig. 3. Full-wave ac-dc rectifier with passive diodes.

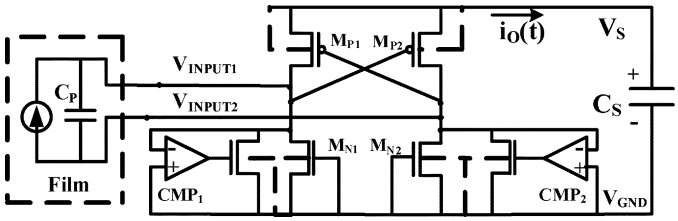

Fig. 4. Proposed hybrid rectifier topology with self-starting up capability.

III. Description of Individual Building Blocks

A. Electrical Model of Piezoelectric Material

Although various physical or mathematical models have been proposed to characterize microscale piezoelectric materials [21], [22], these models are computationally expensive, and incompatible with circuit design and simulation software. Here we use a commonly-used electrical model of piezoelectric thin film for our design [7], [9]–[11]. Fig. 2(a) shows the equivalent electrical model. It consists of a sinusoidal current source that is given by

$$i(t) = I_P \sin(2\pi f t) \tag{1}$$

where I_P depends on the vibration magnitude, size and material of the film, f is the vibration frequency, C_P and R_P are the internal capacitance and resistance of the film, respectively. C_P is almost constant under a wide range of vibration frequencies. This was verified by actual measurements using commercial piezoelectric elements. R_P is usually very large and can be treated as infinite in practice. The output voltage of a piezoelectric film under vibration thus depends on the film's geometry, the piezoelectric properties, the mechanical vibration level, and the output load.

A 1.3 cm × 2.5 cm piezoelectric film with $C_P = 0.5$ nF was used to conduct experiments for verifying this model. The film was mounted on a vibration platform and measurements were conducted for vibration frequency ranging from 0 to 200 Hz. Various resistive loads (R_{LOAD}) were connected to the film and the peak-to-peak output voltages (V_O) were recorded. Based on the electrical model shown in Fig. 2(a) and (1), we have

$$V_o = I_P \frac{R_{\mathrm{LOAD}}}{\sqrt{1 + (2\pi f C_P R_{\mathrm{LOAD}})^2}}. \tag{2}$$

The simulation data and measured data for $f = 60$ Hz are shown in Fig. 2(b), and we verified that the model fits well with the measurement data. In the rest of this paper, we use this electrical model for analysis and optimization.

B. Energy Harvester

Since the piezoelectric element outputs ac current, an ac-dc rectifier is employed to convert the ac current to a dc voltage for supporting the applications. Fig. 3 shows the schematic of a full-wave rectifier using a passive diode bridge. A large storage capacitor C_S $(C_S \gg C_P)$ is used to keep the output voltage V_S essentially constant. Let ΔV be the forward voltage drop of a diode. In [9], large amplitude vibrations were applied and the rectified output voltage V_S reached tens of volts. Thus, the diode voltage drop could be ignored and the passive rectifier was almost exhibiting its ideal behavior. However, for low amplitude vibrations, the output voltage of the rectifier is usually only a few volts (e.g., 2–6 V) that is comparable to the diode voltage drop. Therefore we have to take this voltage drop into account. Based on the work in [9], we derive the average harvested power of the energy harvester $\langle P(t) \rangle$ and the corresponding output voltage V_S at the maximum power point as

$$\langle P(t) \rangle = \frac{2 I_P V_S}{\pi} - 4 V_S^2 f C_P - 8 V_S f C_P \Delta V \tag{3}$$

$$V_{S,\mathrm{OPTIMAL}} = \frac{I_P}{4\pi f C_P} - \Delta V. \tag{4}$$

From (3), it is noted that the passive diode rectifier suffers from a significant harvested power loss due to the last term. Several active ac-dc rectifiers have been proposed to reduce the voltage drop and power loss [16], [18]. Le *et al.* designed an active diode that is composed of a large pMOS transistor and a comparator [16]. However, an external 3.3 V voltage supply is required for the comparator. Therefore, this design is not suitable for battery-less applications since they are not capable of self-starting up. To further reduce the rectifier voltage drop, Lam *et al.* presented a pMOS cross-coupled, nMOS active-diode rectifier with an advanced reverse current control technique for RF wireless applications [18]. However, in vibration energy harvesting systems, since the generated ac current has a much lower frequency than that in RF harvesting systems, the active diodes in vibration harvesting systems can be turned on and off completely without the use of reverse current control. Therefore, it is not necessary to implement the reverse current control technique in our target micro-power systems.

In this work, we propose a hybrid ac-dc rectifier as shown in Fig. 4, which combines passive and active rectifiers together. The terminal voltages of the piezoelectric film are denoted as V_{INPUT1} and V_{INPUT2}, respectively, in Fig. 4. The passive rectifier is used for self-starting up, while the active diode kicks in to replace the passive diode after the energy harvester has

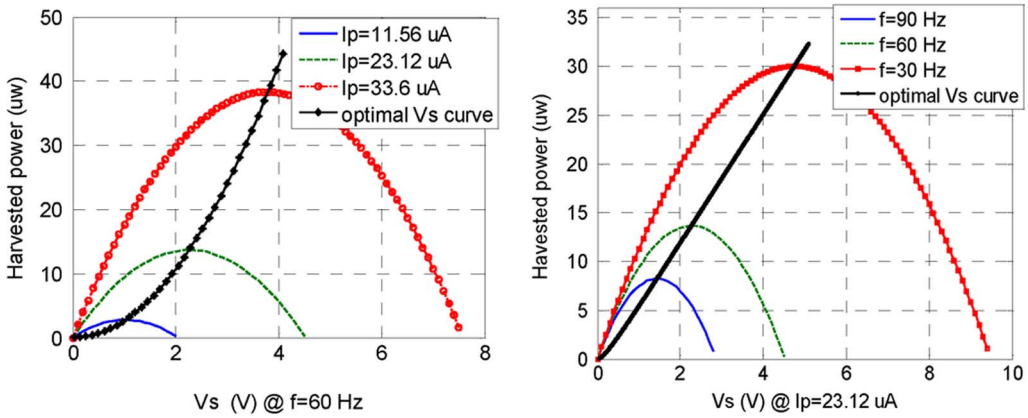

Fig. 5. Simulated MPP voltage varying with vibration statuses.

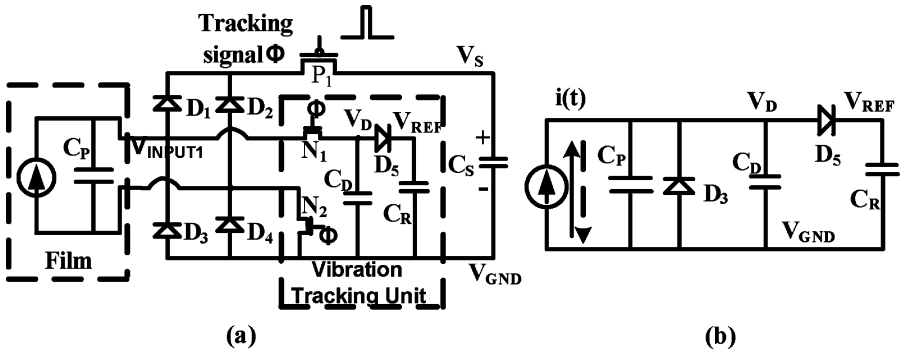

Fig. 6. (a) Time-multiplexed structure for the energy harvester and the tracking unit. (b) Vibration tracking mode when Φ keeps high.

started up. Each active diode is realized by an nMOS transistor and an ultra low power comparator. The startup scenario begins when the piezoelectric film starts to vibrate and generate ac current. Initially V_S is zero and is unable to activate the comparators $(\mathrm{CMP}_1, \mathrm{CMP}_2)$. Thus the active diodes are not working. At this time, the pMOS cross-coupled, nMOS diode-connected passive rectifier operates and provides ac-dc rectification. The current generated from the piezoelectric film charges up C_S through the passive rectifier and V_S starts to increase. When V_S reaches a voltage level that can enable the operation of the comparators, the active rectifier is activated. The active diode will bypass the diode-connected nMOS (M_{N1} and M_{N2}) and eliminate the voltage drop (i.e., $\Delta V = 0$), hence it achieves a higher output power from the energy harvester. Let the current consumption of both comparators be I_{CMP}, then the maximum harvested power and the corresponding optimal output voltage are given by

$$\langle P(t)\rangle = \frac{2I_p V_S}{\pi} - 4V_S^2 f C_P - I_{\mathrm{CMP}} V_S \tag{5}$$

$$V_{S,\mathrm{OPTIMAL}} = \frac{I_P}{4\pi f C_P}. \tag{6}$$

To minimize the power overhead of the active diodes, the comparators are designed to operate in sub-threshold region with very low static current. The detailed circuit structures and design considerations will be discussed in the later sub-section. From (6), we can see that the optimal voltage for maximum power harvesting depends on the vibration magnitude I_P and frequency f, which vary with the deployment environment and time. Thus, the maximum power point changes with the vibration status. To illustrate the above analysis, we simulated the harvested power with different vibration statuses and the results are shown in Fig. 5. It is noted that the optimal V_S value varies significantly. To obtain the maximum harvested power $\langle P(t)\rangle$, we need to track this optimal voltage point with very little power overhead.

C. Vibration Tracking Unit

Vibration status usually does not change very fast and it is not necessary to track the vibration status continuously. As discussed in Section II, a time-multiplexing strategy is employed for energy harvesting and vibration tracking.

Fig. 6(a) shows the detailed circuit implementation of the time multiplexing structure. The vibration tracking unit is composed of two switches N_1, N_2, a diode D_5, and two capacitors C_D and C_R. When the tracking pulse Φ is low, the energy harvesting process is activated. In this mode, the transistors N_1 and N_2 are turned off. Hence the vibration tracking unit is isolated from the piezoelectric film. Meanwhile, the transistor P_1 is turned on. The piezoelectric film is connected to the rectifier and charges the storage capacitor C_S. When the tracking pulse goes high, the tracking unit is connected to the piezoelectric film and the vibration tracking process is activated. To reduce the power overhead of the vibration tracking, we use a very low duty cycle tracking pulse so that most of the time the film is harvesting power through the rectifier.

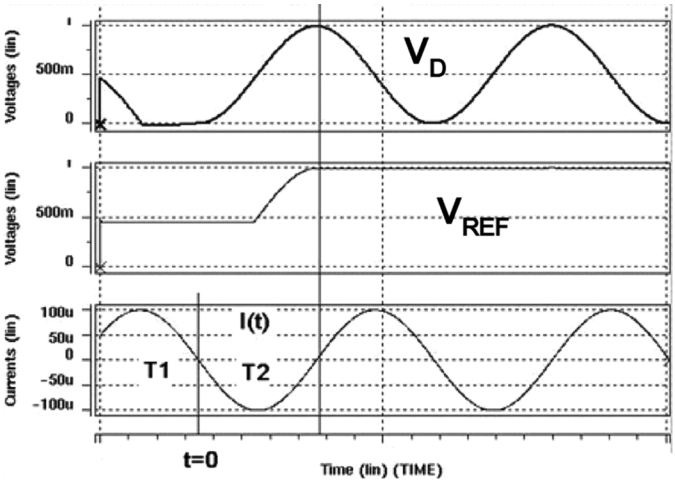

Fig. 7. Simulated waveforms for the vibration tracking process.

The equivalent circuit during the vibration tracking process is shown in Fig. 6(b). Suppose initially the direction of the piezoelectric current flow is along the dashed line shown in Fig. 6(b). C_P and C_D are discharged, and finally V_D decreases to zero and is prevented from decreasing further due to the active diode D_3 which is then forward biased. In the next half cycle, the direction of the current flow is reversed. C_P and C_D are charged up again until V_D reaches its peak value. This positive peak value is maintained as $V_{\rm REF}$ by the capacitor C_R and the active diode D_5, which is similar to the active diode used in the ac-dc rectifier. Fig. 7 shows the simulated waveforms of V_D, $V_{\rm REF}$ and $i(t)$ during the vibration tracking process. During the time period T1, the piezoelectric current discharges C_D. V_D is dropped to zero and maintained at this value by the active diode D_3. Then, in the next half cycle T2, the current reverses its flow direction, and V_D is increased again. At the end of T2, V_D reaches its positive peak value which is maintained as $V_{\rm REF}$.

Let us denote the time instant that $i(t)$ starts to reverse the flow direction as $t = 0$. The relationship between V_D and $i(t)$ is expressed as

$$C\frac{dV_D(t)}{dt} + \frac{V_D(t)}{R_P} = I_P \sin(2\pi ft). \tag{7}$$

By solving this equation, V_D is given by

$$V_D(t) = \frac{I_P}{2\pi fC}\sin\left(2\pi ft - \frac{\pi}{2}\right) + \frac{I_P}{2\pi fC}e^{-t/R_PC} + V_D(0)e^{-t/R_PC}. \tag{8}$$

Here C is the sum of C_P and C_D. $V_D(0)$ is zero at $t = 0$ as described above. Since R_P is very large and R_PC is also very large, e^{-t/R_PC} is very close to 1. The peak value of V_D occurs at $t = T/2$, where T is the cycle time of the environmental vibration and is approximated by

$$V_{D,\rm PEAK} = V_D(t) = \frac{I_P}{\pi fC} \text{ at } t = T/2. \tag{9}$$

If C_D is equal to 15 C_P, we have $V_{\rm REF} = V_{D,\rm PEAK} = 0.25\,V_{S,\rm OPTIMAL}$. The time needed for the piezoelectric current to reverse the flow direction is at most one vibration cycle. In addition, a half cycle is needed to obtain the positive peak value of V_D. Therefore, the minimum duration that the tracking unit needs to be connected to the piezoelectric film (i.e., the pulse width of the tracking signal Φ) is 1.5 T.

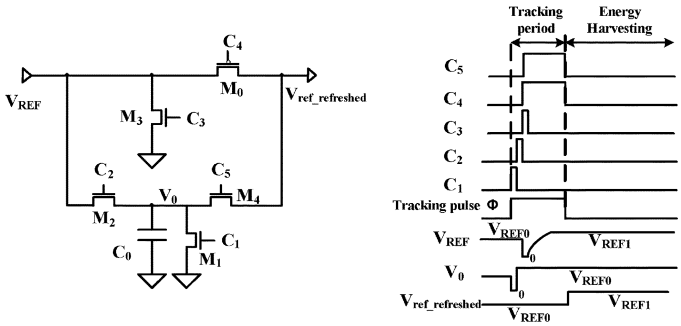

Fig. 8. Refreshing circuit schematic and associated control signals.

D. Refreshing Unit

A refreshing unit is located between the tracking unit and the control unit. It is used to periodically refresh the previously stored reference voltage $V_{\rm REF}$ and provide a new refreshed voltage $V_{\rm ref\_refreshed}$ to the control unit. As shown in Fig. 6, $V_{\rm REF}$ is maintained by the capacitor C_R and $V_{\rm REF}$ can be updated only through the active diode D_5. When the vibration becomes weaker, the peak value of V_D is smaller and D_5 is switched off. Thus, $V_{\rm REF}$ keeps the previous value and cannot be lowered to reflect the new vibration status. Therefore, we need some circuit to refresh the value $V_{\rm REF}$ so that the correct $V_{\rm REF}$ is obtained at each tracking.

Fig. 8 shows the proposed refreshing unit, which consists of five MOS transistors and an on-chip capacitor C_0. Fig. 8 also shows the sequence of control signals that turn on/off these transistors. When a new tracking starts, M_2 is on and charge sharing occurs between C_R and C_0. C_0 is chosen to be much smaller than C_R and hence the voltage at C_0 is very close to $V_{\rm REF}$. Note that the control signal for M_2 is driven by V_S which is about 4 times higher than $V_{\rm REF}$ and hence there is no threshold voltage drop across the switch M_2. Before the charge sharing action, C_0 is discharged to 0 by the switch M_1, which is driven by C_1. After the charge sharing is completed, the output of the refreshing unit is connected to C_0 through M_4. C_R is cut off from the output. A signal C_3 is generated to turn on M_3 to discharge C_R. After C_R is discharged, it is ready for another tracking update. The tracking pulse width is 2T and the above action occurs in the first 0.5 T. This leaves enough time for C_R to be charged up to a new $V_{\rm REF}$. When the tracking process finishes, the tracking pulse Φ returns to zero. $V_{\rm REF}$ is updated and kept by C_R. The output of the refreshing unit is connected back to C_R through M_0 and disconnected from C_0 by turning off M_4.

E. Tracking Pulse Generator

The duty cycle of the tracking pulse directly affects the time that the piezoelectric material can be used for energy harvesting. As a result, the duty cycle should be kept as low as possible. Since the vibration frequency varies with the environment, it is a design challenge to generate a tracking pulse signal with a fixed duty cycle, while at the same time consumes very low power. In this design, we propose to use the ac signal output

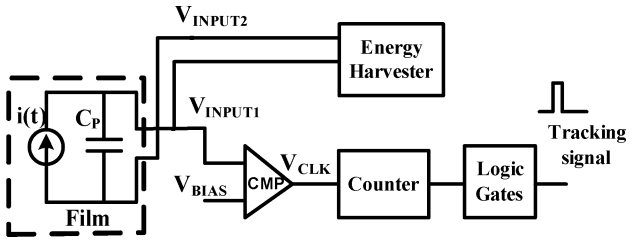

Fig. 9. Block diagram of the tracking pulse generator.

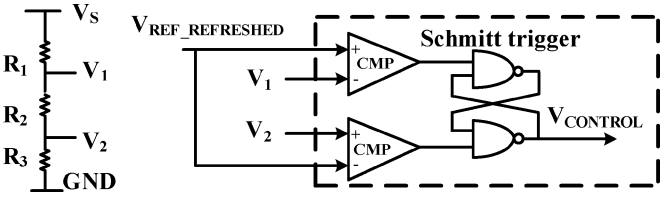

Fig. 10. Block diagram of the control unit.

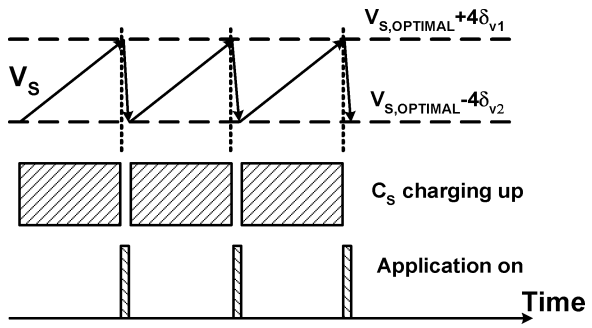

Fig. 11. System operation in a steady state through band-band control.

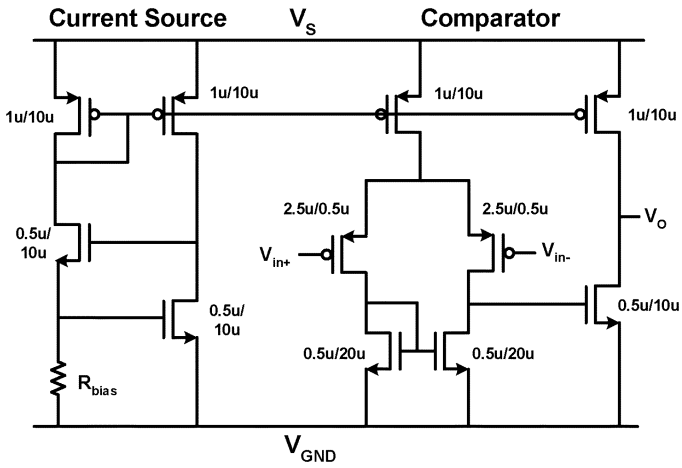

Fig. 12. Voltage independent current source and comparator.

from the piezoelectric material to generate the tracking pulse signal as shown in Fig. 9. One terminal of the piezoelectric film is fed into a voltage comparator and compared with a dc reference voltage $V_{\rm BIAS}$ generated by a bandgap reference and a resistor divider. A clock-like signal $V_{\rm CLK}$, which has the same frequency as that of the ambient vibration, is available at the output of the comparator. A digital counter and combinational logic gates are used to produce a tracking pulse with a fixed duty cycle of 1/64, i.e., around 1.56%. In addition, a tracking pulse width of 2 T is guaranteed to satisfy the minimum requirement of 1.5 T for normal tracking.

F. Control Unit

The control unit is a voltage band-band controller that maintains the output voltage V_S of the energy harvester to around 4 times of $V_{\rm ref\_refreshed}$. It consists of a Schmitt trigger as shown in Fig. 10. A resistor string is used to provide V_1 and V_2 to the control unit. V_1 and V_2 are designed to be $0.25V_S + \delta v_1$ and $0.25V_S - \delta v_2$, respectively. Here δv_1 and δv_2 are two small voltage values and their specific values are not critical for the band-band control. Fig. 11 illustrates the system operation in the steady state. When C_S is charged up to $4V_1$, which is equal to $V_{S,\rm OPTIMAL} + 4\delta {\rm v}_1$, $V_{\rm CONTROL}$ becomes low and turns on S_1. It will trigger the application to wake up from the sleep mode and start an atomic operation (e.g., sensing, data compression, and RF transmission). Power is then transferred to the load. When V_S is lower than $4V_2$ (i.e., $V_{S,\rm OPTIMAL} - 4\delta {\rm v}_2$), $V_{\rm CONTROL}$ becomes high and turns off S_1. Power transfer to the application is stopped and one operation cycle is finished. Later, when the harvested power charges up C_S and V_S reaches $V_{S,\rm OPTIMAL} + 4\delta {\rm v}_1$, the above described operation cycle repeats again.

The speed of the control unit does not need to be very high and low power consumption is the most important design factor. The comparators are operated in sub-threshold region, and its schematic is shown in Fig. 12. It contains a two-stage operational amplifier and a current source, where the bias current remains constant even when the supply voltage V_S changes. Thus, it guarantees that the static bias current of the comparator is small enough for normal sub-threshold operation, even when the supply voltage changes in a wide range (e.g., 2–6.5 V). The operating current for each comparator is 60 nA. The unity-gain bandwidth is in the kilohertz range and open loop gain is around 45 dB.

G. Power Efficiency Discussion

In this section, we discuss the relationship between the power harvesting efficiency and the vibration status. Here we only consider the available electrical power when we calculate the power efficiency and the efficiency of mechanical to electrical power conversion is not included. The definition of power harvesting efficiency is expressed as

$$\eta = \frac{\text{Maximum Available Power}-\text{System Power Loss}}{\text{Maximum Available Power}} = 1 - \frac{\text{System Power Loss}}{\text{Maximum Available Power}}. \quad (10)$$

System power loss mainly consists of the dynamic power loss of the control block and refreshing unit, the static power loss of the current source and comparators, and the duty cycling power loss of the vibration tracking. Note that no energy harvesting is performed when the tracking pulse is high. Let C_E denote the effective load capacitance, f_E the average operation frequency,

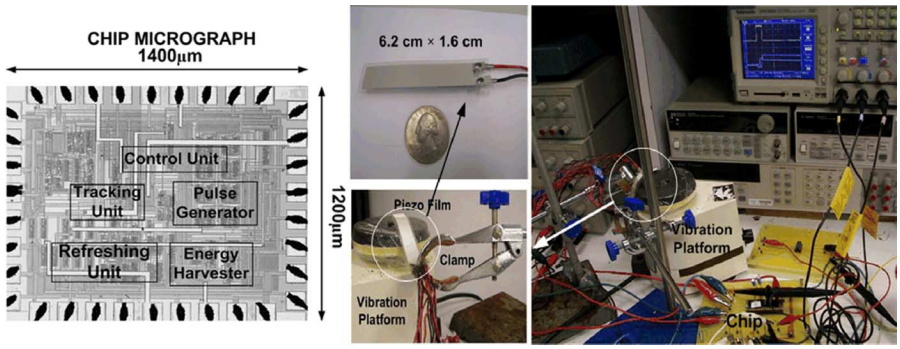

Fig. 13. Chip micrograph and chip measurement setup.

I_S the system static current, and α the duty cycle of vibration tracking. The system power loss can be modeled as

$$P_{\text{SYSTEM LOSS}} = C_E f_E V_{S,\text{OPTIMAL}}^2 + I_S V_{S,\text{OPTIMAL}} + \alpha \langle P(t) \rangle. \tag{11}$$

Substituting the (6) into (5) and neglecting the last term of (5), we can model the maximum available power and the system power loss as

$$P_{\text{AVAILABLE POWER}} = \frac{I_P^2}{4fC_P\pi^2} = 4fC_P V_{S,\text{OPTIMAL}}^2 \tag{12}$$

$$P_{\text{SYSTEM LOSS}} = C_E f_E V_{S,\text{OPTIMAL}}^2 + I_S V_{S,\text{OPTIMAL}} + 4\alpha f C_P V_{S,\text{OPTIMAL}}^2 \tag{13}$$

and (10) becomes (14), shown at the bottom of the page.

In this design, the static power loss is much smaller than the dynamic power loss due to the use of sub-threshold techniques for the comparators. Hence, the above approximation is reasonable. Equation (14) indicates that if the duty cycle α is fixed (e.g., 1.56%), the power harvesting efficiency η is a function of the vibration frequency f, and is independent of the vibration magnitude (I_P). When the same vibration magnitude is applied, a higher vibration frequency results in a higher power harvesting efficiency. This finding will be validated by the experimental measurement results in Section IV.

IV. Experimental Results

The proposed micropower vibration energy harvesting system was designed and fabricated in an AMS 0.35-μm CMOS process, and the micrograph is shown in Fig. 13. The active area including pads is 1.68 mm^2. To mimic the operation environment for measuring the performance of the system, a vibration platform that can provide variable vibration frequency and magnitude was set up, as shown in Fig. 13. Measurements were taken using a Tektronix TPS 2024 Oscilloscope. A stack of piezoelectric films with dimension of 6.2 cm $\times$ 1.6 cm was used for the piezoelectric conversion. These films were experimentally verified with the electrical model discussed in Section III-A. The measured capacitance (C_P) of the stack of films was 33.3 nF. C_S should be much larger than C_P to keep V_S essentially stable, and C_D should be 15 times of C_P and C_R should be much smaller than C_D. Thus the values of these capacitors used in the system are as follows: $C_S = 94$ μF, $C_D = 500$ nF and $C_R = 4.7$ nF. These capacitors are too large to be implemented on chip and so off-chip capacitors are used. Load configuration 1 (shown in Fig. 1) was used in the measurements and one several kilo-Ohm resistor was used as the application load.

To verify the self-starting up capability, we periodically turned on and off the vibration platform. Fig. 14(a) shows the measured output voltage of the energy harvester. The vibration platform was initially turned on and the system operated correctly. Then, the vibration platform was turned off and no power was available for energy harvesting. It is observed that V_S was discharged gradually to ground. Later, when the vibration platform was turned on again, the system automatically started up and entered the stable operation state again. Fig. 14(a) shows that the system is capable of self-starting and can be used in battery-less energy harvesting system.

We also measured the output voltage of the proposed hybrid ac-dc rectifier under different input sinusoidal voltages. Fig. 14(b) shows the measured output voltages of the passive and the hybrid rectifiers versus the input voltage. The passive rectifier suffers from a voltage drop between its input peak voltage and the rectified output voltage. The hybrid rectifier successfully kicks in and bypasses the passive rectifiers when the input voltage is higher than 1.8 V. Here 1.8 V is the minimum operation voltage for the active diodes, because of the relatively high threshold voltage of MOS transistors in the 0.35-μm process and the specific current source structure shown in Fig. 12. If V_S is lower than 1.8 V, the current source is unable to operate normally, and so the active diode is not activated. From Fig. 14(b), we observe that the output voltages of the hybrid rectifier are 0.5 V higher than that of the passive

$$\eta = 1 - \frac{C_E f_E V_{S,\text{OPTIMAL}}^2 + I_S V_{S,\text{OPTIMAL}} + 4\alpha C_P f V_{S,\text{OPTIMAL}}^2}{4C_P f V_{S,\text{OPTIMAL}}^2} = 1 - \alpha - \frac{C_E f_E + \frac{I_S}{V_{S,\text{OPTIMAL}}}}{4C_P f} \approx 1 - \alpha - \frac{C_E f_E}{4C_P f} \tag{14}$$

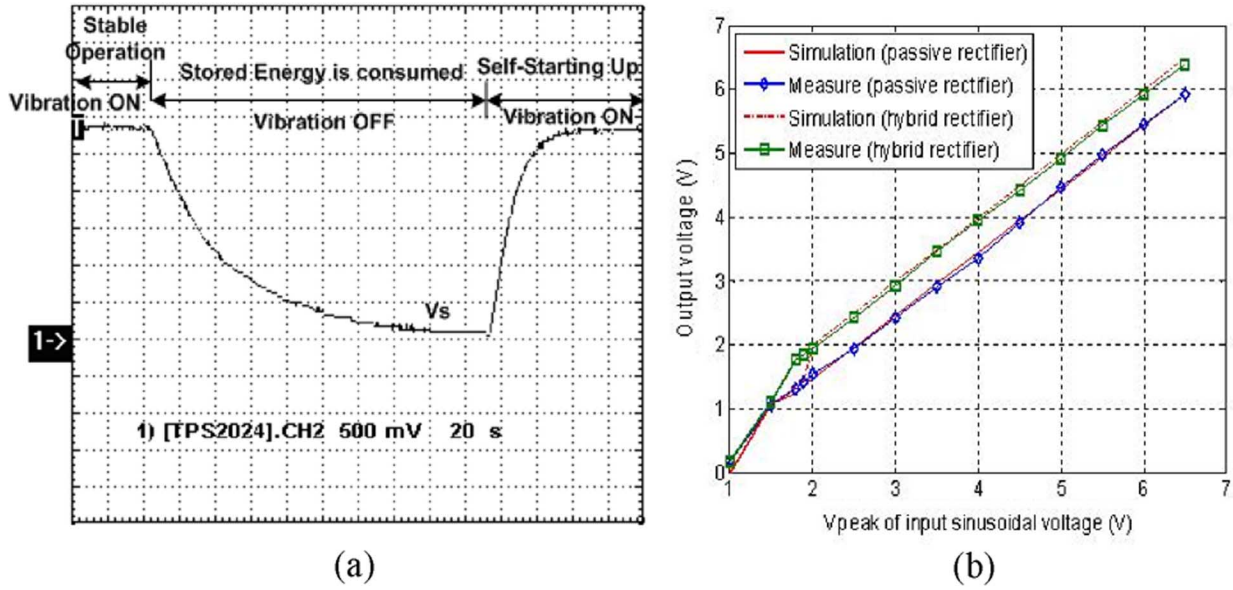

Fig. 14. (a) Measurement result of system self-starting up process. (b) Output voltage comparison between the passive rectifier and our hybrid rectifier.

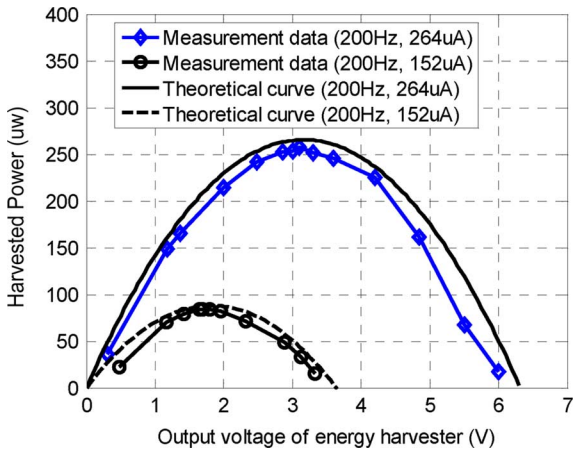

Fig. 15. Power harvesting characteristics.

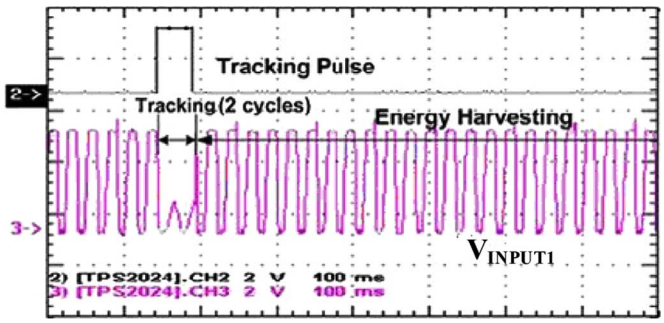

Fig. 16. Time-multiplexed vibration tracking.

rectifier, which means the proposed rectifier has a much smaller voltage drop, and hence more harvested power.

The power harvesting characteristics of the overall system was measured for two sets of vibration statuses ($I_P = 152\ \mu$A, $f = 200$ Hz) and ($I_P = 264\ \mu$A, $f = 200$ Hz) and then compared with the harvested power model expressed in (4). The harvested power was measured for different resistive loads by directly connecting the load to the output of the rectifier. For each load, we measured V_S and the corresponding power consumed by the resistive load, and the results are plotted in Fig. 15. The theoretical power harvesting curves, modeled by (5), are also plotted in Fig. 15 for comparison. Note that the theoretical curve assumes ideal condition and does not consider actual system or circuit implementation, so it does not have any power overhead. Fig. 15 shows that the measurement results follow closely with the model in (5) and the measured optimal voltage point matches well with the theoretical one. The difference between the two sets of curves is mainly due to the power overhead (i.e., conduction loss, switching loss, and the active rectifier power overhead) of the ac-dc rectifier.

We carried experiments to demonstrate the function and effectiveness of the proposed vibration tracking scheme. Fig. 16 shows the measurement results of the time-multiplexing tracking strategy. The generated tracking pulse has a width of two vibration cycles, and during this short tracking time, the piezoelectric films are connected to the vibration tracker to get the optimal voltage value. When the tracking pulse becomes low, the piezoelectric films are connected to the ac-dc rectifier for energy harvesting.

The function of the vibration tracking unit was measured and demonstrated. The measured waveforms are shown in Fig. 17. In this measurement, the applied vibration frequency was around 50 Hz and when the tracking pulse arrived, the vibration tracking unit started to operate. During this short tracking time (i.e., 2T), the peak value of V_D was correctly captured and stored as $V_{\rm REF}$ through an active-diode.

Fig. 18 shows the measurement results for the tracking pulses and $V_{\rm ref\_refreshed}$. Before the system completely starts up, no tracking pulse is generated and $V_{\rm ref\_refreshed}$ is kept at ground. Once the first tracking pulse arrives, the vibration tracker starts to work and $V_{\rm ref\_refreshed}$ is updated at that time.

The reference tracking for varying vibration magnitude and frequency were also measured. We first used a constant vibration frequency of 20 Hz and changed the vibration strength from

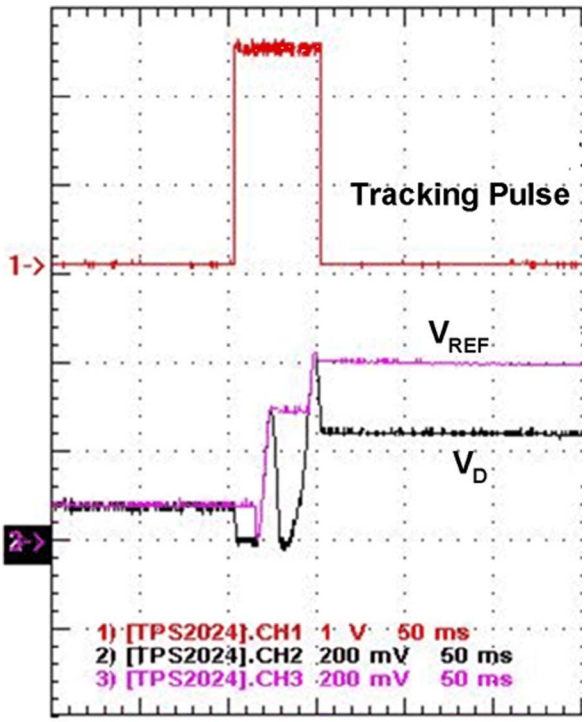

Fig. 17. Measured waveforms of vibration tracking unit.

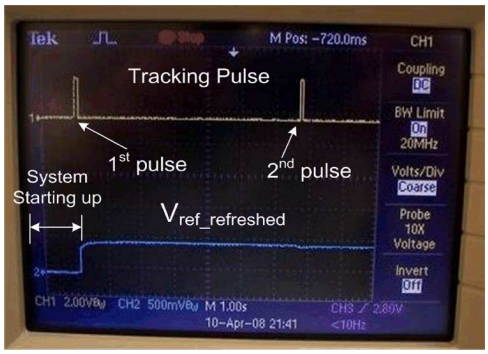

Fig. 18. Measured waveforms for vibration tracking when system starts up.

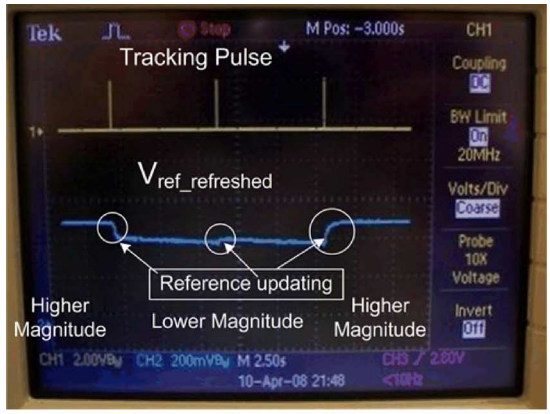

(a)

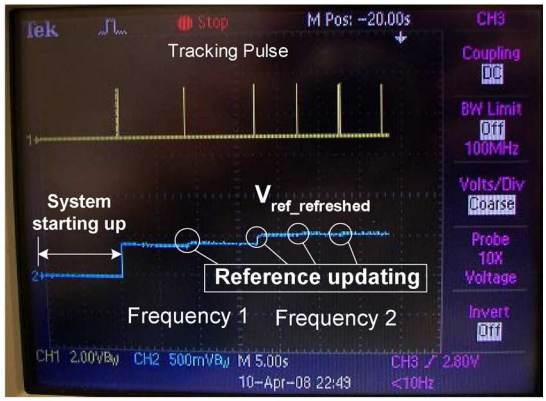

(b)

Fig. 19. Measured waveforms for vibration tracking process.

high to low and then back to high. A low vibration frequency was used for this measurement because it was easier to capture the changes in the waveforms in the oscilloscope during the measurement. The reference voltage was correctly generated as shown in Fig. 19(a). Next, we tuned the vibration platform to change the vibration frequency from 16 to 20 Hz. The vibration status was tracked and the reference voltage was updated accordingly for different frequencies. The waveform is shown in Fig. 19(b).

Finally, we measured the power harvesting efficiency. For a particular vibration status, we define the power harvesting efficiency as the ratio of the power available to the load using the vibration tracker over the maximum power available to the load. Different sets of vibration statuses were used for the measurement. For each set of vibration status, the maximum power available to the load was achieved by using the corresponding optimal matching resistive load as shown in Fig. 15, while turning off the tracking and control blocks. The power available to the load using the vibration tracker was obtained by enabling the MPP tracking control blocks and providing an arbitrary non-optimal resistor as the load and then measuring the actual power consumed by the load. Fig. 20 shows the results for different sets of vibration statuses. In using the vibration tracker, the output voltage of the harvester can be maintained at a value very close to the theoretical MPP value. It shows that the proposed scheme tracks well with the change in vibration statuses. The corresponding power harvesting efficiency of the proposed MPPT scheme is also shown in Fig. 20. The measured efficiency is well above 90%. It shows that the power overhead of the vibration tracker and the control block is very low. The efficiency is about 93% for 100 Hz vibration and 96% for 200 Hz vibration, respectively. This measurement result validates our analysis and prediction shown by (14).

We also compared the proposed low-overhead MPP tracking scheme with fixed voltage band-band control scheme in [8]. Two vibration statuses, (200 Hz, 152 μA) and (200 Hz, 264 μA) were measured and the corresponding harvested power values and efficiencies are summarized in Table I. In this comparison, three different fixed voltages were used for the voltage band-band control scheme, namely 1.8, 2.5, and 3.2 V, respectively. Compared with the fixed voltage control, the efficiency of the proposed MPP tracking scheme is about the same when the fixed voltage is also the optimal voltage for that particular vibration status. It has about 8%–70% of improvement in efficiency for the cases when the fixed voltages are not the optimal

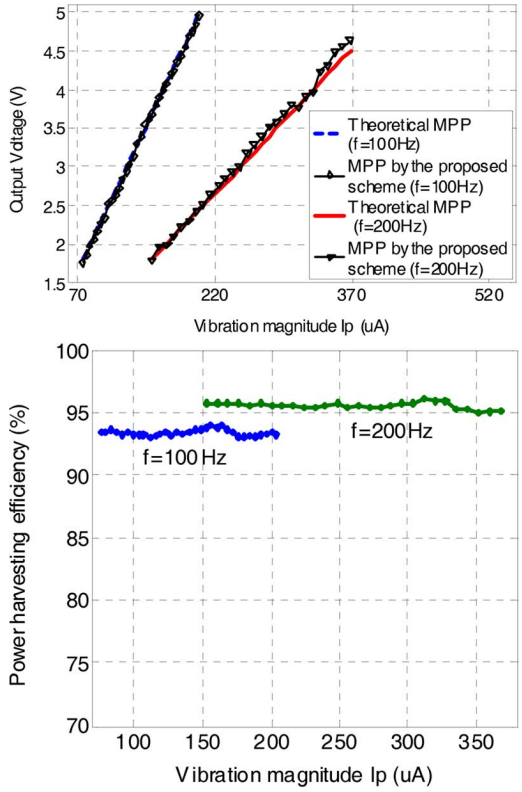

Fig. 20. Vibration tracking performance and efficiency.

TABLE I
TRACKING PERFORMANCE OF THE PROPOSED MPPT SCHEME

Vibration Statuses	*200Hz, 152μA*	*200Hz, 264μA*
Theoretical optimal V_s	1.8V	3.2V
V_s obtained using vibration tracker	1.8V	3.28V
Theoretical maximum harvested power	88.0μW	265μW
Actual harvested power and efficiency using vibration tracker	84.2μW 95.8%	254μW 95.6%
Actual harvested power and efficiency using fixed voltage band-band control with V_s=1.8V	86.5μW 98.3%	175μW 66.0%
Actual harvested power and efficiency using fixed voltage band-band control with V_s=3.2V	21.0μW 23.9%	261μW 98.2%
Actual harvested power and efficiency using fixed voltage band-band control with V_s=2.5V	60.9μW 69.2%	232μW 87.5%

voltage. This shows the advantage of the proposed MPP tracking scheme. Also, the power overhead of the MPPT scheme is small.

V. CONCLUSION

We present a low-overhead vibration power scavenging system for ultra low power ubiquitous applications. This system is capable of self-starting up without other power source. A novel MPP tracking scheme with very low power overhead was presented. The circuit was fabricated and measurements were carried out to verify the tracking performance and the feasibility of the proposed platform. Measurement results show that the power harvesting efficiency of the overall circuitry is higher than 90%.

REFERENCES

[1] J. Rabaey, J. Ammer, T. Karalar, S. Li, B. Otis, M. Sheets, and T. Tuan, "PicoRadios for wireless sensor networks: The next challenge in ultra-low-power design," in *IEEE ISSCC Dig. Tech. Papers*, 2002, pp. 200–201.

[2] B. A. Warneke and K. S. J. Pister, "An ultra-low energy micro-controller for smart dust wireless sensor networks," in *IEEE ISSCC Dig. Tech. Papers*, 2004, pp. 316–317.

[3] S. Y. Lee and S. C. Lee, "An implantable wireless bidirectional communication microstimulator for neuromuscular stimulation," *IEEE Trans. Circuits Syst. I, Reg. Papers*, vol. 52, no. 12, pp. 2526–2538, Dec. 2005.

[4] L. Mateu and F. Moll, "Review of energy harvesting techniques and applications for microelectronics," in *Proc. SPIE Microtechnol. New Millennium*, 2005, pp. 359–373.

[5] S. Roundy, P. K. Wright, and J. Rabaey, "A study of low level vibrations as a power source for wireless sensor nodes," *Comput. Commun.*, vol. 26, no. 11, pp. 1131–1144, 2003.

[6] S. Roundy, P. K. Wright, and J. Rabaey, *Energy Scavenging for Wireless Sensor Networks with Special Focus on Vibrations*. Norwell, MA: Kluwer, 2004.

[7] Measurement Specialties, USA, "Technical manual for piezoelectric film," 2008. [Online]. Available: http://www.meas-spec.com

[8] E. S. Leland, E. M. Lai, and P. K. Wright, "A self-powered wireless sensor for indoor environment monitoring," presented at the Wireless Network. Symp., Austin, TX, 2004.

[9] G. K. Ottman, H. F. Hofmann, A. C. Bhatt, and G. A. Lesieutre, "Adaptive piezoelectric energy harvesting circuit for wireless remote power supply," *IEEE Trans. Power Electron.*, vol. 17, no. 5, pp. 669–676, May 2002.

[10] G. K. Ottman, H. F. Hofmann, and G. A. Lesieutre, "Optimized piezoelectric energy harvesting circuit using step-down converter in discontinuous conduction mode," *IEEE Trans. Power Electron.*, vol. 18, no. 2, pp. 696–703, Mar. 2003.

[11] E. Lefeuvre, D. Audigier, C. Richard, and D. Guyomar, "Buck-boost converter for sensorless power optimization of piezoelectric energy harvester," *IEEE Trans. Power Electron.*, vol. 22, no. 5, pp. 2018–2025, Sep. 2007.

[12] E. Lefeuvre, A. Badel, C. Richard, and D. Guyomar, "High-performance piezoelectric vibration energy reclamation," in *Proc. SPIE Int. Symp. Smart Struct. Smart Mater.*, Mar. 2004, vol. 5390, pp. 379–397.

[13] S. Ben-Yaakov and N. Krihely, "New resonant rectifier for capacitive sources," in *Proc. 23rd IEEE Conv. Electr. Electron. Eng.*, Sep. 2004, pp. 48–51.

[14] E. Lefeuvre, A. Badel, C. Richard, and D. Guyomar, "Piezoelectric energy harvesting device optimization by synchronous electric charge extraction," *J. Intell. Mater. Syst. Struct.*, vol. 16, pp. 865–876, Oct. 2005.

[15] L. Chao, C. Y. Tsui, and W. H. Ki, "A batteryless vibration-based energy harvesting system for ultra low power ubiquitous applications," in *Proc. ISCAS*, 2007, pp. 1345–1352.

[16] T. Le, J. Han, A. V. Jouanne, K. Mayaram, and T. S. Fiez, "Piezoelectric micro-power generation interface circuits," *IEEE J. Solid-State Circuits*, vol. 41, no. 6, pp. 1411–1420, Jun. 2006.

[17] S. Xu, K. D. T. Ngo, T. Nishida, G. B. Chung, and A. Sharma, "Converter and controller for micro-power energy harvesting," in *Proc. 20th Annu. Appl. Power Electron. Conf. Expo.*, 2005, vol. 1, pp. 226–230.

[18] Y. H. Lam, W. H. Ki, and C. Y. Tsui, "Integrated low-loss CMOS active rectifier for wirelessly powered devices," *IEEE Trans. Circuits Syst. II, Exp. Briefs*, vol. 53, no. 12, pp. 1378–1382, Dec. 2006.

[19] K. K. Tse, M. T. Ho, S. H. Chung, and S. Y. Hui, "A novel maximum power point tracker for PV panels using switching frequency modulation," *IEEE Trans. Power Electron.*, vol. 17, no. 6, pp. 980–989, Nov. 2002.

[20] C. Alippi and C. Galerti, "An adaptive system for optimal solar energy harvesting in wireless sensor network nodes," *IEEE Trans. Circuits Syst.*, vol. 55, no. 6, pp. 1742–1750, Jul. 2008.

[21] A. Erturk and D. J. Inman, "Issues in mathematical modeling of piezoelectric energy harvesters," *Smart Mater. Structures*, vol. 17, no. 065016, p. 14, 2008.

[22] A. Erturk and D. J. Inman, "An experimentally validated bimorph cantilever model for piezoelectric energy harvesting from base excitations," *Smart Mater. Structures*, vol. 18, no. 025009, p. 18, 2009.

Chao Lu (S'07) received the B.S. degree in electrical engineering from the Nankai University, Tianjin, China, and the M.S. degree from the Department of Electronic and Computer Engineering, Hong Kong University of Science and Technology, Hong Kong, in 2004 and 2007, respectively. He is currently pursuing the Ph.D. degree from Purdue University, West Lafayette, IN.

His research interests include design and analysis of micro-scale energy harvesting systems, power management integrated circuits for ultra low power applications, and device and architecture co-design of low temperature poly silicon thin film transistors.

Mr. Lu was a recipient of the Best Paper Award of the International Symposium on Low Power Electronics and Design (2007).

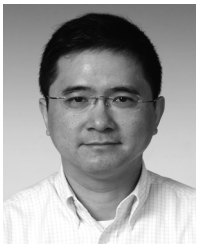

Chi-Ying Tsui (M'94) received the B.S. degree in electrical engineering from the University of Hong Kong, Hong Kong, and the Ph.D. degree in computer engineering from the University of Southern California, Los Angeles, in 1994.

He joined the Department of Electrical and Electronic Engineering, Hong Kong University of Science and Technology, Hong Kong, in 1994, where he is currently an Associate Professor. His research interests include designing VLSI architectures for low power multimedia and wireless applications, developing power management circuits and techniques for embedded portable devices and ultra-low power systems. He has published over 150 referred technical journal and conference papers.

Prof. Tsui was a recipient of the Best Paper Awards from the IEEE TRANSACTIONS ON VERY LARGE SCALE INTEGRATION (VLSI) SYSTEMS (1995), International Symposium on Low Power Electronic and Design (2007), IEEE International Symposium on Electronic Design Test and Applications (2008), and supervised the Best Student Paper Award of the 1999 IEEE ISCAS. He also received the Design Awards in the IEEE ASP-DAC University Design Contest in 2004 and 2006.

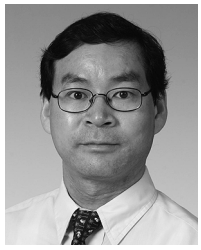

Wing-Hung Ki (S'86–M'91) received the B.Sc. degree from the University of California, San Diego, in 1984, the M.Sc. degree from the California Institute of Technology, Pasadena, in 1985, and the Engineer and Ph.D. degrees from the University of California, Los Angeles, in 1990 and 1995, respectively, all in electrical engineering.

In 1992, he joined the Department of Power and Battery Management, Micro Linear Corporation, San Jose, CA, as a Senior Design Engineer, where he worked on the design of power converter controllers. In 1995, he joined the Hong Kong University of Science and Technology, Hong Kong, where he is currently a Professor with the Department of Electronic and Computer Engineering. His research interests include design and analysis of switch-mode power converters, charge pumps, low-dropout regulators band-gap references; power management for microsensor and RFID applications; and analog IC design methodologies.

Prof. Ki was a recipient of the Outstanding Design Award (2004) and the Special Feature Award (2006) of the LSI University Design Contest organized by Asia and South Pacific Design Automation Conference, and the Best Paper Award of the International Symposium on Low Power Electronic and Design (2007) and the International Symposium on Integrated Circuits (2009).